Propagation of Short Electron Pulses in a Plasma Channel

N. Barov,[1] M. E. Conde,[1] W. Gai,[2] and J. B. Rosenzweig[1]
[1]*Department of Physics and Astronomy, University of California, Los Angeles, 405 Hilgard Avenue, Los Angeles, California 90095*
[2]*High Energy Physics Division, Argonne National Laboratory, 9700 South Cass Avenue, Argonne, Illinois 60439*
(Received 28 April 1997)

We report the near-steady-state propagation over long distance of a 25 psec, tightly focused relativistic electron beam which creates, by radial ejection of plasma electrons, a focusing ion channel in a plasma of electron density smaller than the beam. A dense beam core, close in radius to the injected beam, which was nearly matched to the ion focusing strength, is observed at the plasma exit. Time-resolved imaging confirms that this core is situated in the trailing half of the beam, as predicted by analytical and computer models. We discuss the impact of these results on plasma wake field acceleration schemes. [S0031-9007(97)04922-3]

PACS numbers: 52.40.Mj, 52.35.Mw, 52.75.Di

When a tightly focused electron beam propagates in an underdense plasma (beam density greater than the plasma electron density, $n_b > n_0$), the plasma electrons are expelled radially by the space charge of the beam, forming an ion channel which in turn provides a uniform, linear focusing force on the beam. Beam propagation over long distances in this ion-focused regime has been studied experimentally [1] in the context of beams long compared to the plasma skin depth [2] (radian of plasma wave oscillation), $\sigma_z \gg k_p^{-1}$. For short beams ($\sigma_z < 2k_p^{-1}$), which are of interest as drivers for plasma wake field acceleration (PWFA) [3], previous work on beam self-focused propagation in plasma has been confined to a study in which transverse equilibration was observed in an overdense ($n_b < n_0$) plasma [4]. There has also been significant theoretical and experimental interest in thin [5,6] and thick [7] plasma lenses, primarily for linear collider final focus applications, but with no experimental results yet obtained in the underdense regime.

The present experiments were motivated by the proposed use of the underdense ("blow-out") regime for PWFA [8], which is very attractive in terms of drive and accelerating beam guiding. In contrast to the overdense case, when an ion column free of plasma electrons is formed, the focusing due to this column is predicted to be linear in radius r and independent of longitudinal position z. The blow-out regime also promises high quality acceleration fields inside the electron-free region, composed of uniform phase fronts which are dependent only on z. The present experiments were begun to better understand the initial studies of PWFA in this regime [9] at the Argonne Wakefield Accelerator Facility (AWA) [10]. In these studies, beam parameter (current, emittance, and energy) requirements for obtaining ion channel self-focusing are difficult to satisfy [11]. This is especially true for short beams, as the electrons near the leading edge (head) of the pulse receive less focusing due to the finite response time of the plasma electron motion. If the beam is initially β matched to the focusing gradient of an ion channel [11] (initial depth of focus of the incoming beam waist at plasma entrance $\beta = \sigma_r^2/\varepsilon$ is $\beta_{\mathrm{eq}} = \sqrt{\gamma/2\pi r_e n_0}$; σ_r and ε are the rms beam radius and emittance, respectively) the transverse distribution in the body of the beam is nearly stationary, while that near the head expands radially. The loss in beam head density associated with this expansion further retards the plasma electron response, causing the pinch point (where sufficient focusing develops to stabilize the beam radius) to move backwards in the beam frame. The relaxation distance for these beam head dynamics, in which a near equilibrium is established, is $4\beta_{\mathrm{eq}} \cong 5$ cm in the present experiments, or less than half of the plasma length, $L_p = 12$ cm. After relaxation, emittance-driven beam head erosion proceeds at a much slower pace [11,12]. These focusing effects are best observed when the fractional beam energy loss is small; it is 0.16 for the $\leq$20 MeV/m deceleration wake fields predicted for the present measurements. Theoretical work also predicts a beam centroid instability due to transverse dipole wake fields [13] (electron hose instability), but computer simulations indicate this instability is much suppressed for $k_p \sigma_z < \pi$ [14].

The plasma chamber used in the experiments is shown in Fig. 1, with electron pulses derived from the AWA [10] entering from the left. The AWA is an rf photoinjector which currently produces an $E = 14.5$ MeV beam ($\gamma = E/m_e c^2$) with a high charge Q per bunch and short pulse length σ_z appropriate for wake field studies. Beam diagnostics immediately upstream of the plasma chamber include an energy spectrometer, an emittance measurement system, an integrating current transformer (ICT) and Faraday cup to measure Q, a phosphor screen and, at the focal point of the β-matching solenoid, an optical transition radiation (OTR) screen to obtain transverse beam profile images. The bunch length is measured using a Cerenkov radiation diagnostic at the end of the plasma, as described below.

The plasma is created by a dc hollow cathode arc discharge. The arc current density in the beam region is 4 orders of magnitude smaller than the beam current density, and thus does not significantly affect the beam's transverse

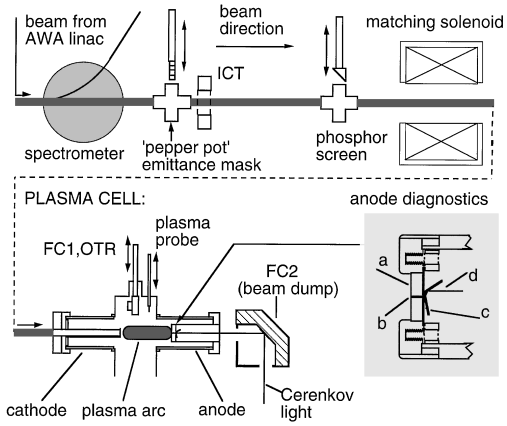

FIG. 1. Diagnostics beam line and plasma cell (shown without the plasma radial confinement solenoid). The anode diagnostics include (*a*) tungsten collimator with (*b*) 1 mm wide slit, (*c*) 500 μm thick quartz Cerenkov plate, and (*d*) mirror and outgoing light.

motion. The plasma density ($\sim$25% ionization fraction), which is in the region of $n_0 = 1.15 \times 10^{13}$ cm^{-3}, is mapped with a Langmuir probe (calibrated with a 140 GHz microwave interferometer), and found to be within 10% of the peak value over the nominal plasma length, with a steep initial ramp near the cathode tip. The half-maximum point, located 9 mm downstream of the cathode, is $L_p \cong$ 12.25 cm away from the diagnostic-filled anode. The plasma density is typically measured at the start and finish of a one hour experimental run.

The bunch parameters Q, σ_r, β, and ε at the beginning of the plasma cannot be measured while the plasma is on, and thus are not simultaneously measured along with the beam's final state under the influence of plasma focusing. These quantities are also measured before and after the plasma run, to eliminate the possibility of a drift in accelerator conditions. The plasma focusing experiments demand that Q be measured for every shot using the upstream nondestructive ICT, at which point the charge is larger than that propagating in the plasma chamber, due to a small amount of scraping by the cathode assembly aperture. This scraping fraction is quantified under plasma-off conditions by simultaneous measurements with the ICT and FC1, the Faraday cup following the cathode. The initial focal spot size near the waist of the β-matching solenoid was measured with plasma off at the OTR screen at FC1. Some of these profiles deviated significantly from the cylindrical symmetry assumed in the simulations, having an asymmetric shape with an aspect ratio as high as 4:1. The 25% of the shots having an asymmetry larger than 2:1 were rejected, and the remaining images tested for peak intensity as well as for fractional integrated intensity inside a test radius of 0.28 mm. A symmetric Gaussian with $\sigma_x = \sigma_y = \sigma_r$, having the same integral defines an effective radius, which was found to be nearly independent of Q, with mean value of $\sigma_r = 284 \pm 24$ μm. The presence of mild asymmetries causes use of the effective σ_r to underestimate the peak beam density, predicting $n_b/n_0 = 2.0$ at 14 nC (assuming a 25 psec FWHM bunch length, see below). The actual value from the peak intensity in the image data is $n_b/n_0 = 2.0$ and 2.5 at $Q = 7$ and 14 nC, respectively, and the plasma is well underdense at beam input for all experimental conditions.

The beam divergence $\sigma_{x'}$ and bunch length were measured with plasma off using the anode diagnostics, including a 1 mm wide (4 mm deep) tungsten slit aperture followed by a 0.5 mm thick quartz plate inclined 12° to the beam direction. A portion of the radially polarized outgoing Cerenkov light from this diagnostic (transverse resolution is 80 μm) exits the plate at the Brewster angle to suppress internal reflections and is sent to either a CCD camera for time-integrated imaging or to the 2 psec resolution streak camera. The beam charge after collimation by the slit aperture is recorded on the Faraday cup following the anode, FC2. For measuring $\sigma_{x'}$, the beam is allowed to drift from the initial waist to the anode. The divergence is calculated from the width of a Gaussian fit to the profile along the slit, and the drift length from the initial waist (the error in the waist location can be up to 6 mm, causing a 5% error in $\sigma_{x'}$). The beam divergence is 18.5 mrad at 14 nC and decreases linearly to 15.5 mrad at 7 nC, yielding $\varepsilon_n \cong \gamma\varepsilon = 149$ and 130 mm mrad and initial $\beta_i =$ 1.52 and 1.74 cm, for high and low charge, respectively. These emittance values also agree with upstream pepper-pot measurements. Note that the input beam β function is slightly mismatched in these cases to the ion focusing $\beta_{\text{eq}} = 1.25$ cm. The input bunch length is measured by refocusing the beam on the anode, with the Cerenkov light analyzed with a Hamamatsu C1587 streak camera, giving a pulse length of 25 $\pm$ 3 psec FWHM.

After the beam is collimated, the transmitted charge Q_{trans} is recorded on the downstream Faraday cup FC2, and the value multiplied by a factor of 1.25 to correct for the charge scraped by the anode wall after multiple scattering in the 130 μm thick Cu exit foil and quartz plate. With plasma focusing, the fraction of the initial charge transmitted through the slit, $\eta = Q_{\text{trans}}/Q$, serves as an independent measure of the beam radius.

With the plasma on, the time-integrated Cerenkov profile shown in Fig. 2 displays a narrow, intense peak as a result of ion focusing. The x-projected FWHM in this case is 0.9 mm, 40% broader than at the plasma start, but consistent with the beam head spreading predicted by simulations. The projected peak intensity is 10 times greater than in the no plasma case, and is accompanied by a reduction in intensity at large $|x|$, away from the peak. As the beam transverse centroid jitter [15] is not small compared to the slit aperture, a large shot-to-shot spread in η due to increased scraping appears. To select only shots centered on the slit, a shot is rejected if its y peak (defined by the 0.8-maximum points) is within 100 μm of one, but not both, apertures. Values of η selected in this way for an initially matched ($z_0 = 0$) case are displayed in Fig. 3, along with the results of simulations. Varying the value

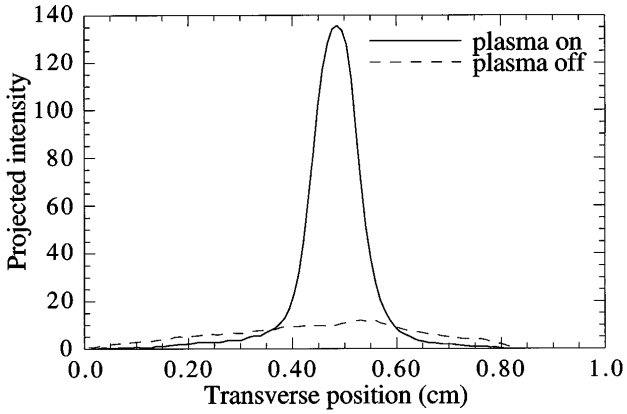

FIG. 2. Transverse beam profile after collimation, from digitized CCD camera image of Cerenkov light.

of $\sigma_{x'}$ in the simulations within expected errors produces η values 3% higher and 7% lower than nominal; even so, the measured η includes points falling far below this range, especially for lower Q. For these points we cannot experimentally rule out possible double-peaked y profiles. Some of the spread in the data also certainly arises from fluctuations in the initial beam aspect ratio. An initially strongly asymmetric beam profile would cause plasma electrons to blow out only in the narrow dimension, giving enhanced focusing in this dimension, thus producing further profile asymmetry. In any case, it can be stated that a large η ensures a vertically well slit-centered distribution which is approximately symmetric.

The simulation results given in Fig. 3 use the plasma fluid code NOVO [7], modified to include a super-particle representation of the beam electrons [9]. Results of this code have been benchmarked against an electromagnetic particle-in-cell (PIC) code; the calculation of η is nearly identical (smaller in NOVO by 4%), and so NOVO was used in this analysis because of its speed. The calculations use 8000 beam particles, initialized to a thermal distribution derived from the measured beam size and divergence.

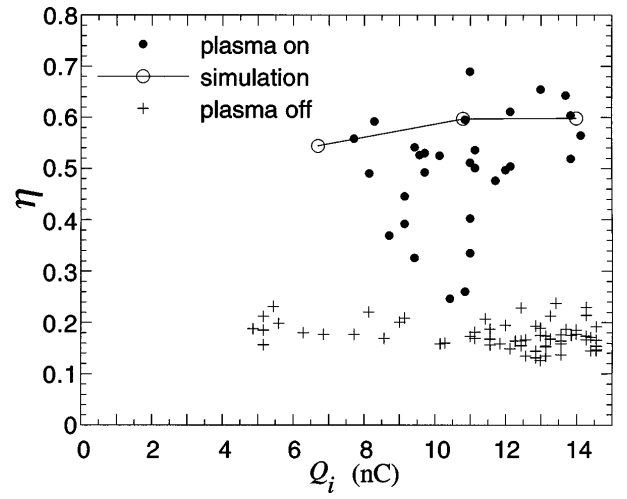

FIG. 3. Transmission data and simulations for an initially nearly β-matched case.

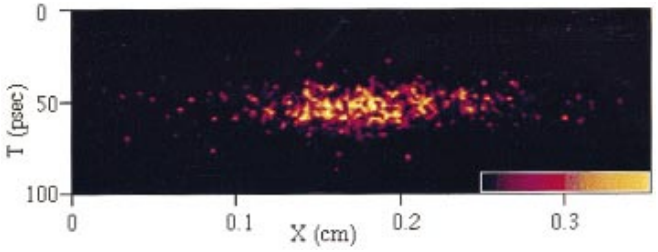

FIG. 4(color). False-color Cerenkov streak image showing $n_b(x,t)$, with earlier times (beam head) on top, and yellow representing the highest value.

A more detailed view of the underlying dynamics is offered by the time-resolved streak camera images which, however, contain information only about longitudinal and horizontal profiles, as measured in a 20 μm vertical strip centered in the slit aperture. Adequate beam symmetry and vertical centering in the slit were insured in these measurements by requiring $\eta \geq 0.45$. A streak image satisfying this test is shown in Fig. 4, a false color image of the distribution $n_b(x, y = 0, t)$. The predicted flaring of the beam head can be observed in this image. No streak image of the plasma-off case is shown, since beam expansion causes the intensity to drop below useful levels.

Each image that was analyzed further was sliced into short (5.7 psec) t slices; for every t slice the integrated (in x) intensity, as well as the beam width, defined as the region containing half the integrated intensity ($-x_{1/2} \leq x \leq x_{1/2}$), were determined. As the streak images at this resolution are inherently noisy, the results of this analysis for ten images within a narrow charge window ($10.2 < Q < 11.8$ nC) were summed to produce a composite picture of the beam distribution. This is shown in Fig. 5, along with the rms error bars and PIC simulation results, analyzed to give beam width as a function of t slice. The experimental data and PIC simulations display a profile flared at the beam head due to radial expansion, as well as a beam core which is nearly matched and slightly larger, $\sigma_r \cong 370$ μm, due to adiabatic antidamping of the emittance,

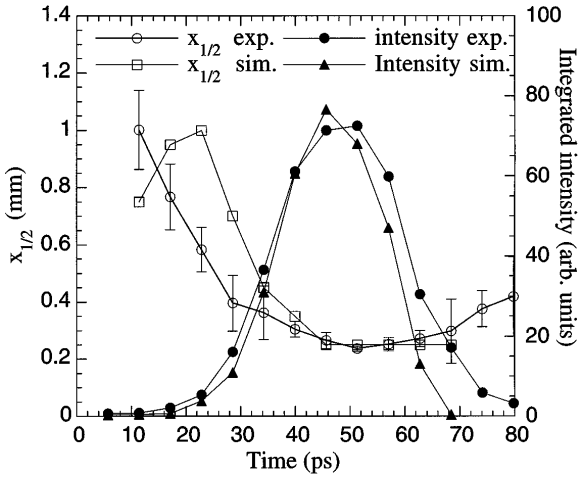

FIG. 5. Time-slice dependence of beam intensity and half-width, from experiment (exp.) and PIC simulation (sim.).

than at input. The simulation's agreement with the data is quite good, with a notable deviation in that the experimental results generally show less pronounced beam-head expansion, except for one leading simulation point—this value of $x_{1/2}$ is obtained from very few beam simulation particles, and is therefore subject to unphysical statistical fluctuations. The larger expansion in the simulated beam-head behavior may be due to the assumption of an input beam with a thermal transverse phase space. This is not accurate for photoinjector beams, where the emittance of a t slice is smaller than that of the full beam, with much of the total emittance arising from a correlation between t and orientation of transverse phase space [16]. We note finally that the time-resolved measurements show no significant evidence for onset of electron-hose instability.

The above data were taken with beams nearly β matched to the focusing channel strength. In order to explore dynamics of mismatched beams further, data runs were taken with the input beam focused to a waist 2.5 cm upstream of the plasma column start, so that is was strongly mismatched in both β and $d\beta/dz$. This case, with n_0 unchanged, displayed a smaller spread in η than seen in Fig. 3, with values ranging from 0.27 to 0.59; the average was $\eta = 0.42 \pm 0.01$ (with plasma-off, $\eta = 0.1$), while simulation results were in the range of $\eta = 0.45$ to 0.52. Further, η for these mismatched beams was observed for several different values of n_0, a test which serves to distinguish the difference between the case $n_b < n_0$, where the focusing has negligibly weak dependence on n_0, and the case $n_b > n_0$, where the envelope oscillations proceed at twice the ion-channel betatron frequency, $k_{\mathrm{env}} = 2k_\beta \equiv 2/\beta_{\mathrm{eq}} \sim \sqrt{n_0}$. Several measures of the η distribution in these runs are shown as a function of n_0 in Fig. 6: peak, 80th percentile, and mean. All of these quantities are sensitive to n_0, with strong suppression of transmission occurring where focusing phase advance $k_{\mathrm{env}} L_p$ gives a local minimum beam size at the plasma exit. This sensitivity is a signature that $n_b > n_0$ over significant lengths of the plasma.

In conclusion, short intense relativistic bunches derived from an rf photoinjector have been observed, through integrated and time-dependent imaging, as well as collimator transmission, to self-guide in an underdense plasma for lengths many times the initial β. Picosecond-resolution imaging of transverse beam distribution displays the equilibrium body and trumpet-shaped head predicted by simulations and analysis [11,12]. The simulations are in quantitative agreement with the beam sizes and transmissions obtained for symmetric beams in the experiment, with the observed deviations likely arising from the approximate nature of the beam simulation model. The simulation results predict stable beam guiding which continues over longer distances, as must be the case for their effective use as underdense PWFA drivers [8,11]. Our results also point to a problem which must be addressed in future PWFA work: stabilizing the transverse beam centroid and distribution shape. This will be accomplished

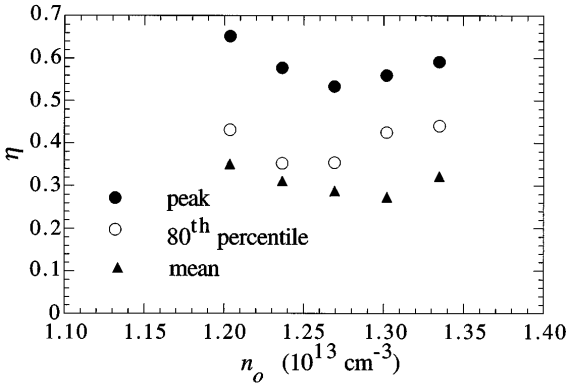

FIG. 6. Dependence of η distribution measures (peak, 80th percentile, and mean) as a function of n_0 for β-mismatched case.

through advances in laser (e.g., spatial filtering) and photocathode (e.g., high quantum efficiency, uniform emitter such as Cs_2Te) technology. Additionally, for refined predictions of PWFA performance, further development of the beam-plasma interaction computational model, including three-dimensional effects, would be useful.

The authors would like to thank E. Colby, A. Murokh, P. Schoessow, and J. Simpson for aid and advice along the way. This work was supported by the U.S. Department of Energy Grant No. DE-FG03-93ER40796 and Grant No. W-31-109-ENG-38, and the Alfred P. Sloan Foundation Grant No. BR-3225.

[1] W. E. Martin *et al.*, Phys. Rev. Lett. **54**, 685 (1985).
[2] This quantity is commonly defined in the theory of intense relativistic beam-plasma interaction; see, e.g., H. Uhm and G. Joyce, Phys. Fluids B **3**, 1587 (1991).
[3] P. Chen *et al.*, Phys. Rev. Lett. **54**, 693 (1985); J. B. Rosenzweig *et al.*, Phys. Rev. Lett. **61**, 98 (1988).
[4] J. B. Rosenzweig *et al.*, Phys. Fluids B **2**, R1586 (1990).
[5] J. J. Su *et al.*, Phys. Rev. A **41**, 3321 (1990).
[6] G. Hairapetian *et al.*, Phys. Rev. Lett. **72**, 1244 (1994); H. Nakanishi *et al.*, Phys. Rev. Lett. **66**, 177 (1991).
[7] P. Chen *et al.*, Phys. Rev. D **40**, 923 (1989); J. B. Rosenzweig *et al.*, Phys. Rev. D **39**, 2039 (1989).
[8] J. B. Rosenzweig *et al.*, Phys. Rev. A **44**, R6189 (1991).
[9] N. Barov *et al.*, in *Proceedings of the 1995 Particle Accelerator Conference, Dallas, 1995* (IEEE, New York, 1996), p. 631.
[10] P. Schoessow *et al.*, in *Proceedings of the 1995 Particle Accelerator Conference* (Ref. [9]), p. 976.
[11] N. Barov and J. B. Rosenzweig, Phys. Rev. E **49**, 4407 (1994).
[12] J. Krall *et al.*, Phys. Fluids B **1**, 2099 (1989).
[13] D. Whittum *et al.*, Phys. Rev. Lett. **67**, 991 (1991).
[14] J. Krall and G. Joyce, in *Advanced Accelerator Concepts*, AIP Conf. Proc. No. 335 (AIP, New York, 1995), p. 505.
[15] Space-charge dominated beams from photoinjectors display strong steering due to laser-photocathode pointing errors, as the applied focusing is stronger than for a single particle. The off-set centroid, which behaves as a single particle, is overfocused, leading to enhanced steering.
[16] X. Qiu *et al.*, Phys. Rev. Lett. **76**, 3723 (1996).